

# EFFECTS OF PARTICLE SIZE ON DRAINAGE QUALITY FROM THREE LITHOLOGIES<sup>1</sup>

Kim A. Lapakko, Jennifer N. Engstrom, and David A. Antonson<sup>2</sup>

**Abstract.** Samples of three different waste-rock lithologies (olivine norite, diatrema, and adularized mudstone) were selected to determine the relationship between particle size and acid production for each of three lithologies. The three samples were characterized with respect to chemistry, mineralogy, and petrology. Five to six particle size fractions from each lithology were subjected to dissolution testing for typical periods of 335 to 465 weeks. The dependences of (1) drainage pH, (2) time of dissolution prior to drainage acidification, (3) fraction of Ca and carbonate minerals reacted prior to drainage acidification, and (4) relative rates of acid production and neutralization on particle size varied among the three rock types. For example, drainage pH values from fine fractions of the olivine norite decreased more rapidly than those from coarse fractions, while the opposite trend was observed for the adularized mudstone. Drainage pH values from the diatrema presented a third trend, with no strong dependence of the temporal pH variation on particle size. The dependence of drainage pH and related variables on particle size was due to the influence of particle size reduction on the relative abundance of exposed acid-producing and acid-neutralizing mineral surface areas. This influence is dependent on minerals present in waste rock, their grain size, and occurrence, and must be considered in interpretation of kinetic test results and modeling these results for field application.

**Additional key words:** mine drainage, acid drainage, ARD, drainage quality prediction, waste rock, kinetic testing, diatrema, olivine norite, mudstone

---

<sup>1</sup>Poster paper presented at the 7<sup>th</sup> International Conference on Acid Rock Drainage (ICARD), March 26-30, 2006, St. Louis MO. R.I. Barnhisel (ed.) Published by the American Society of Mining and Reclamation (ASMR), 3134 Montavesta Road, Lexington, KY 40502

<sup>2</sup>Kim A. Lapakko is a Principal Engineer and Jennifer N. Engstrom is a Mineland Reclamation Specialist at the Minnesota Department of Natural Resources, Division of Lands and Minerals, St. Paul, MN 55105-4045. David A. Antonson is a Mineland Reclamation Field Supervisor at the Minnesota Department of Natural Resources, Division of Lands and Minerals, Hibbing, MN 55746

7<sup>th</sup> International Conference on Acid Rock Drainage, 2006 pp 1026-1050

DOI: 10.21000/JASMR06021026

## Introduction

Kinetic testing is one tool used for the prediction of acid release from waste rock. In these tests, waste-rock samples are subjected to dissolution in the laboratory and drainage quality observed is used to predict the acid nature of drainage from waste rock in the field. This concept has been likened to metallurgical testing of drill core samples to predict metal recovery from an ore body (Lapakko 1990). However, mine-waste drainage quality prediction may be more complicated than metallurgical testing due to, among other factors, the long time over which mine-waste drainage quality is of concern (Lapakko 1990).

Particle size reduction is often necessary for predictive dissolution testing of waste rock. Unfortunately the quality of drainage, in particular drainage pH, from small waste rock particles may not accurately simulate the quality of drainage from operational scale waste rock. Iron sulfide oxidation and Ca/Mg carbonate mineral dissolution are responsible, respectively, for the generation and neutralization of acid. The rates of these reactions are generally proportional to the surface area of the respective mineral available for reaction. Particle size reduction may result in preferential enhancement of acid-producing or acid-neutralizing mineral surface areas. This in turn will affect the relative rates of acid generation and acid neutralization and, consequently, the drainage pH.

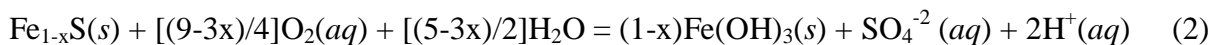
Thus, the experiment presented here examines the effects of waste rock particle size on drainage quality. These lithologies were selected based on preliminary indications that they would provide different particle size dependencies. Five to six particle size fractions of three waste rock samples were subjected to dissolution at approximately 25°C to determine the influence of particle size on mine-waste drainage pH.

## Background Chemistry

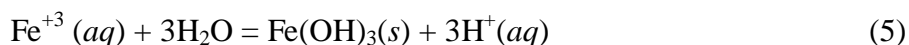
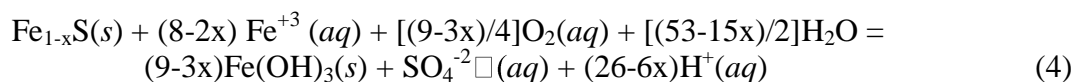
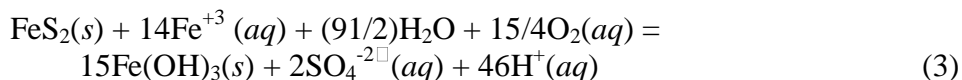
### Acid Generation

The following discussion focuses on mineral dissolution reactions resulting in acid production and acid neutralization that influence acid release from mine waste. Some solid phases of interest in mine-waste characterization are pyrite and pyrrhotite. Detailed discussion of aqueous geochemistry fundamentals and geochemistry of acid mine drainage is presented by Nordstrom (1999), Nordstrom and Alpers (1999), Smith (1999), and Smith and Huyck (1999).

The oxidation of Fe sulfide minerals such as pyrite (FeS<sub>2</sub>) and pyrrhotite (Fe<sub>1-x</sub>S, 0.7 < x < 1.0) is responsible for the majority of acid production by mine wastes (Stumm and Morgan 1981). Reactions 1 and 2 show pyrite and pyrrhotite oxidation by oxygen (after Stumm and Morgan 1981; Nelson 1978) in which acid (H<sup>+</sup>) and sulfate (SO<sub>4</sub><sup>-2</sup>) are released to solution. Sulfate in mine-waste drainage is typically the first indicator of sulfide mineral oxidation. The Fe product is ferric hydroxide, although formation of intermediate aqueous ferric hydroxyl species (e.g. Fe(OH)<sup>+2</sup>(aq), Fe(OH)<sub>3</sub>(aq)) will also result in acid production.



Ferric iron ( $\text{Fe}^{+3}$ ) can also oxidize pyrite and pyrrhotite (reactions 3, 4, respectively). The amount of acid generated as a result of the pyrite or pyrrhotite oxidation by  $\text{Fe}^{+3}$  iron is the same as that for oxidation by oxygen. The additional acid apparently generated in reaction 3 ( $42 \text{ H}^+$ ) is due to precipitation of the aqueous  $\text{Fe}^{+3}$  iron reactant as ferric hydroxide (reaction 5).



The rate of Fe sulfide oxidation and attendant acid production is dependent on solid-phase compositional variables and microbial activity, as well as the availability of oxygen and water. Oxidation rates vary among sulfide minerals, and it is often reported that reactivity decreases in the order marcasite > pyrrhotite > pyrite (e.g. Kwong and Ferguson 1990). However, different reactivity rankings have been reported by other authors and may be a function of reaction conditions, trace element concentrations of the minerals, and crystal-morphology characteristics, among other factors (Jambor 1994; Plumlee 1999). For a given sulfide mineral, the oxidation rate increases with the available surface area. For example, the oxidation per unit mass of framboidal pyrite, with a high associated surface area, is reported to be much more rapid than that of euhedral pyrite (Pugh et al. 1984; White and Jeffers 1994).

Where as the abiotic rate of pyrite oxidation by oxygen decreases slightly as pH decreases, the overall abiotic rate increases as pH decreases into a range where  $\text{Fe}^{+3}$  iron becomes the dominant oxidant (Williamson and Rimstidt 1994). Nordstrom (1982) reported that as “pH decreases to 4.5,  $\text{Fe}^{+3}$  iron becomes more soluble and begins to act as an oxidizing agent.” As pH further decreases, bacterial oxidation of  $\text{Fe}^{+2}$  iron becomes the rate limiting step in the oxidation of pyrite by  $\text{Fe}^{+3}$  iron (Singer and Stumm 1970), which is the only significant oxidizing agent in this pH range (Nordstrom 1982; Singer and Stumm 1970; Kleinmann et al. 1981). In laboratory tests the pyrrhotite oxidation rate in the pH range of 3.5 to 4.05 was roughly six to seven times that in the range of 5.35 to 6.1, and the higher rate was attributed to bacterially mediated oxidation (Lapakko and Antonson 1994). Olson (1991) reported the biotic rate of pyrite oxidation in the approximate pH range of 1.5 to 2.0 in the laboratory was roughly 34 times the abiotic rate. Data presented by Nordstrom and Alpers (1999) suggest that the bacterially mediated rate of pyrite oxidation by  $\text{Fe}^{+3}$  iron is roughly two to three orders of magnitude faster than the abiotic oxidation by oxygen at pH 2.

These weathering reactions produce acidic, Fe- and sulfate-rich waters which can 1) react with sulfide minerals and accelerate their oxidation, 2) evaporate partially or totally to precipitate hydrated Fe-sulfates and other minerals, and/or 3) contact and react with host rock minerals to neutralize some or all of the acid. Acidic flow that is not neutralized within the mine waste will exit as acid rock drainage (ARD).

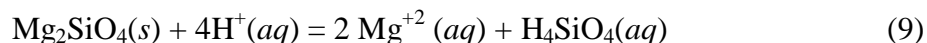
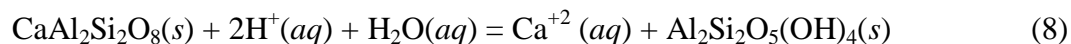
## Acid Neutralization

The balance between the rates of acid production by Fe-sulfide mineral oxidation and host-rock mineral neutralization will determine the acidity of mine-waste drainage. The most effective minerals for neutralizing acid are those containing calcium carbonate and magnesium carbonate, including calcite, magnesite, dolomite, and ankerite ( $\text{CaCO}_3$ ,  $\text{MgCO}_3$ ,  $\text{CaMg}(\text{CO}_3)_2$ , and  $\text{CaFe}(\text{CO}_3)_2$ , respectively). Reaction 6 represents the dominant acid-neutralizing reaction of calcite above pH 6.4, whereas reaction 7 is the dominant reaction below pH 6.4 (Drever, 1988):



Of the carbonate minerals, calcite dissolves most rapidly (Busenberg and Plummer 1986, Rauch and White 1977). Relative to calcite, the rate of dolomite dissolution is about an order of magnitude slower (Busenberg and Plummer 1982) and the rate of magnesite dissolution is about four orders of magnitude slower (Chou et al. 1989). The rate of siderite ( $\text{FeCO}_3$ ) dissolution under anoxic conditions is reported to be three orders of magnitude slower than that of calcite (Greenberg and Tomson 1992). However, Fe and manganese carbonates (e.g. siderite and rhodochrosite,  $\text{MnCO}_3$ ) do not provide net acid neutralization under oxidizing conditions, due to oxidation of the released Fe or manganese, the subsequent hydrolysis and precipitation of these metals, and the consequent acid production.

Dissolution of silicates such as plagioclase feldspars (e.g. anorthite in reaction 8, Busenberg and Clemency 1976) and olivine (e.g. forsterite in reaction 9, Hem 1970) can also neutralize acid. However, their rates of dissolution and consequent acid neutralization are slow relative to the carbonate minerals (Nesbitt and Jambor 1998). For example, White et al. (1999) reported “at near neutral pH, the dissolution rate of calcite is approximately 7 orders of magnitude faster than the dissolution of plagioclase feldspar.” Nonetheless, silicate mineral dissolution can maintain neutral conditions if the rate of acid production is very slow (Lapakko and Antonson 1994; Lapakko et al. 1997; Lapakko and Antonson 2002). The effectiveness of silicate minerals in neutralizing acid increases with increasing mineral surface area that, in turn, increases with increasing mineral content and decreasing grain size.



## Key Solid-Phase Factors Controlling Mineral Oxidation and Dissolution

Whereas the acid producing and acid neutralizing mineral contents, and the balance of these contents, influence mine-waste drainage quality, there are several subtle mineralogical factors which are also influential. Individual minerals may be entirely liberated from the rock matrix, occur interstitial to other minerals (partially liberated or exposed), or as inclusions within other minerals. The extent of mineral surface area exposed affects availability for reaction. For example, acid-producing or acid-neutralizing minerals included within minerals such as quartz will be essentially unavailable for reaction.

Oxidation of sulfide minerals and dissolution of carbonate minerals are surface reactions and, therefore, the rates of these reactions are dependent on the reactive surface area. Reactivity decreases as mineral surfaces are covered with coatings, such as Fe oxyhydroxides, whereas the concentration of lattice defects tends to increase reactivity. Mineral surface area is dependent on the extent to which the mineral is liberated from the rock matrix, mineral grain size, and the “roughness” of the mineral surface. Mineral exposure and grain size can be affected by reducing the particle size of rock fragments, and the effects of such reduction must be considered in mine-waste drainage quality prediction.

### Methods

The rock samples, olivine norite, diatrema, and adularized mudstone<sup>1</sup>, selected for predictive testing were relatively fresh, that is, they were not highly oxidized due to environmental exposure. The norite had been stockpiled in a test pile for about 15 years, but the rock particles collected were fairly large and were crushed prior to distribution for analysis and predictive testing. The diatrema had been in a low-grade stockpile for two to three years and the mudstone had been exposed to the environment for less than two months as blasted waste rock in a mine pit.

The waste rock samples, as received, were all fairly coarse (approximately minus six inches), and were crushed to a nominal minus-one-inch (25.4 mm) size. Size fractions were separated by subjecting rock samples (150-200 g) to 15 minutes on a ro-tap apparatus loaded with U.S. standard mesh sieves. Six size fractions were selected for examination: 1) d # 0.053 mm (-270 mesh), 2) 0.053 < d # 0.149 mm (+270/-100 mesh), 3) 0.149 < d # 0.5 mm (+100/-35 mesh), 4) 0.5 < d # 2.0 mm (+35/-10 mesh), 5) 2.0 < d # 6.35 mm (+10 mesh/-0.25 inch), and 6) 6.35 < d # 19 mm (+0.25/-0.75 inch). After the separation, the various size fractions were wet sieved and dried.

### Analytical Methods

Solid-Phase Chemistry. Solid-phase chemical analyses were conducted by ACME Analytical Laboratories Ltd. in Vancouver, B.C. Total sulfur and carbon were determined by infrared adsorption using a LECO C244 Carbon-Sulfur analyzer. To determine total sulfur, the sample was crushed to -100 µm and heated to >1650 °C. A second split was ignited to 800 °C to decompose sulfides and drive off sulfur as sulfur dioxide and the remaining SO<sub>4</sub><sup>-2</sup> was measured. Sulfur as sulfide was calculated by subtraction. To determine evolved carbon dioxide the sample

---

<sup>1</sup> Identifications of two of the rocks were changed from those used in earlier publications on this experiment. After mineralogic analysis and mode determination, the rocks were renamed using Streckeisen (1976, 1978). The olivine norite (normalized content of 47% plagioclase, 15% orthopyroxene, and 37% olivine) was previously referred to as troctolite-gabbro. The diatrema (normalized content of 71% quartz and 29% potassium feldspar) was referred to as quartz latite. The more detailed information indicated the rock was not quartz latite and was not readily classified based on the aforementioned publications. The rock will be referred to as diatrema based on the mechanism of formation of the rock. The mineral contents are presented subsequently. From this point forward the olivine norite will be referred to as “norite” and the adularized mudstone as “mudstone” for simplicity.

was dissolved in HClO<sub>4</sub> and warmed to 70 °C to release CO<sub>2</sub>. Whole rock chemistry was determined by inductively coupled plasma spectroscopy (ICP; Jarrel Ash AtomCorp Model 975) on a sample crushed to -100 μm, fluxed with LiBO<sub>2</sub>, heated to 1050 °C, and dissolved in HNO<sub>3</sub>.

Aqueous-Phase Chemistry. The drainage quality samples were analyzed on site to determine drainage volume (by weight), pH, alkalinity (if pH  $\geq$  6.3) or acidity, and specific conductance. An Orion SA 720 pH meter, with a Ross combination pH electrode (8165), was used for pH determinations. Alkalinity and acidity were analyzed using standard titration techniques (APHA et al. 1992). A Myron L conductivity meter was used to determine specific conductance.

Samples taken for SO<sub>4</sub><sup>-2</sup> and metals analyses were filtered through a 0.45-micron filter. Sulfate analyses before week 16 were determined at the MN DNR laboratory in Hibbing, MN using an HF Scientific DRT-100 nephelometer for the BaSO<sub>4</sub> turbidimetric method (APHA et al. 1992). Sulfate determinations on samples collected between weeks 16 and 32 were analyzed using ICP, at Midland Research Center. Subsequently, SO<sub>4</sub><sup>-2</sup> concentrations were determined at the Minnesota Department of Agriculture in St. Paul, MN (MDA). Sulfate concentrations exceeding five mg/L were determined using a Technicon AA2 automated colorimeter. Lower concentrations were determined using a Dionex ion chromatograph and, after week 257, a Lachat QuickChem 8000.

Metals samples were acidified with 0.2 mL of ultra-pure HNO<sub>3</sub> per 50 mL sample. Metals analyses before week 32 were conducted at the MN DNR Minerals laboratory in Hibbing, MN using a Perkin Elmer 603 atomic absorption spectrophotometer in flame mode. Subsequent analyses were conducted at MDA. Ca, Mg, Na, and K were determined on a Varian 400 SPECTRAA.

Data were checked by examining concentration variation over time, relationships of concentrations with conductance, and charge balances. Samples for which concentrations were anomalous were reanalyzed. If reanalysis was not possible (e.g., due to inadequate sample volume) the anomalous values were not included in mass release or rates of release calculations.

Mineralogy. Preliminary mineralogical analyses were conducted by Louis Mattson of the Midland Research Center in Nashwauk, MN. X-ray diffraction (XRD; Philips Electronic Instruments Inc.) was used in conjunction with chemical analyses for mineral identification as well as for determination of the approximate modal composition. The CO<sub>2</sub> content was used to determine the total carbonate mineral content. The carbonate minerals present were identified by XRD, and checked by scanning electron microscopy (SEM; Amray model 1200B) and energy dispersive spectroscopy (EDS; Noran Instruments model 2010). For some samples, optical microscopy (standard Zeiss petrographic microscope) was used for additional verification.

Electron microprobe analyses were conducted by Dr. Peter McSwiggen (McSwiggen and Associates, Minneapolis, MN) using a JEOL 8600 electron microprobe (accelerating voltage of 15 kV and beam current of 20 nanoamps). Mineral standards were used for all calibrations. Dr. McSwiggen determined the modal abundance and chemistry of the minerals in the 2.0-6.35 mm size fraction for the diatrema and the norite and both 2.0-6.35 and 6.35-19 mm size fractions of the mudstone. Modal abundance of the other size fractions was determined using (1) the bulk chemistry of the fraction (as determined by ACME Analytical Laboratories, Ltd.) and (2) assuming the mineral chemistry did not vary among size fractions. The degree of sulfide and

carbonate mineral exposure was estimated by comparing the average diameter of mineral grains (determined by microprobe) to that of the rock particles in each size fraction.

### Dissolution Procedure

The <0.053, 0.053–0.149, and 0.149–0.5 mm fractions were placed onto a glass fiber filter and into the upper segment (reactor) of a two-stage filter unit. For the larger size fractions a single-stage, cylindrical, acrylic reactor was used. Additional detail is on both apparatuses and the methods can be found in Lapakko et al. (2004). For particle size fractions finer than 0.5 mm, the sample mass was 75 g and the rinse volume was 200 mL. For the larger particle size samples, the sample mass was 1000 g and the rinse volume was 400 mL. Due to the limited mass of the diatreme available, the 6.35–19 mm fraction of this rock was omitted, and 500 g rather than 1000 g of the 2.0–6.35 mm fraction was used in the experiment and was rinsed with 200 mL.

At the start of the experiment, the solids were rinsed between four and seven times to remove reaction products that had accumulated since the samples were rinsed during sieving. The rinse water was analyzed for specific conductance to provide an indicator of the decreasing masses of oxidation products removed from the solids. Subsequently, the solids were rinsed weekly for 134 to 465 weeks.

Between rinses the solids were stored in the reactors in a room in which temperature and humidity were controlled. Temperature ranged from 21 to 29°C with a mean of 25°C and a standard deviation of 1.2°C. Relative humidity over the same period ranged from 46 to 70 percent with a mean of 58 percent and a standard deviation of 3.4 percent.

Between week 0 and week 1 the reactors were left uncovered and weighed on a daily basis to determine the variation in water retained over time. Due to the wide discrepancy of drying among reactors, it was determined that the covers should be left on the reactors between rinses, except for reactors containing the <0.053 mm fractions of the diatreme and the mudstone, which would not drain under wet conditions. The water remaining on top of these solids was decanted by pipet from the reactor and added to the drainage before analysis. The percentage of the total volume decanted from the <0.053 mm fractions of the diatreme and the mudstone for the first 30 weeks was approximately 62 and 39 percent, respectively. It should be noted that, based on the weekly weights and the presence of moisture on the inside walls of the covered reactors, it was assumed that the relative humidity was near 100 percent.

### Calculations

Acid production ( $AP(S_T)$ ) was determined by multiplying total S by 31.25 to correspond with convention, rather than 31.2 as is more accurate.

For the mudstone and the norite samples, neutralization potential ( $NP[(Ca+Mg)CO_3]$ ) was determined using equation 10. For the diatreme sample however, there were conflicting mineralogical analyses regarding the speciation of the carbonate minerals. The carbonate mineralogy associated with the initial investigation (bulk chemistry, SEM, and XRD) indicated siderite and calcite contents of 3.2 and 0.5 wt %, respectively. The microprobe analyses, however, indicated siderite ( $FeCO_3$ ), rhodochrosite ( $MnCO_3$ ), and/or kutnahorite ( $(Mn,Ca)CO_3$ ) and varying modes of these minerals were present. Four methods were used to determine the

fraction of CO<sub>2</sub> that was associated with the Ca and Mg (Lapakko et al. 2004) and yielded an average value of 27 percent. NP[(Ca+Mg)CO<sub>3</sub>] was then calculated based on CO<sub>2</sub> analyses on each particle size fraction.

$$NP[(Ca+Mg)CO_3] = 10 \times (CaCO_3) + 11.9 \times (\%MgCO_3) \quad (10)$$

The masses of SO<sub>4</sub><sup>-2</sup>, Ca, and Mg released were calculated as the product of the observed concentration in the drainage and the drainage volume and summed to a total mass release for each particle size. For weeks during which concentrations or volumes were not determined, missing values were estimated as the average of previous and subsequent measured values. Average rates of SO<sub>4</sub><sup>-2</sup>, Ca, and Mg release rates were calculated by dividing the respective mass release from week three to the end of the period of record by the number of weeks in this period.

Empirical neutralization potentials (ENP) were calculated to determine the acid-neutralizing mineral dissolution prior to drainage pH decreasing below 6.0 and remaining in this range. The acid-neutralizing mineral dissolution was calculated as the sum of the cumulative Ca and cumulative Mg released (expressed as g CaCO<sub>3</sub> eq kg<sup>-1</sup>) prior to the point at which drainage pH decreased below pH 6. The ratio of ENP to NP[(Ca+Mg)CO<sub>3</sub>] was used to quantify the available NP[(Ca+Mg)CO<sub>3</sub>], that is, the fraction of CaCO<sub>3</sub> and MgCO<sub>3</sub> minerals that dissolved to maintain pH ≥ 6.0. If the pH of drainage from a solid never decreased permanently below 6, the ENP was reported as "greater than" the sum of the total Ca and Mg release for the period of record.

Calcium and Mg can also be released to drainage by dissolution of minerals other than carbonates, such as SO<sub>4</sub><sup>-2</sup>. Therefore, the release during the initial rinse period weeks (weeks zero to two) was excluded from the ENP calculation to account for the fairly rapid release of Ca and Mg from the sulfates.

## **Results and Discussion**

### **Introduction**

Mine-waste drainage pH is strongly influenced by the balance of acid-producing and acid-neutralizing mineral dissolution reaction rates. The rates of these reactions are generally proportional to the respective mineral surface areas available for reaction, as opposed to the entire mineral surface area present. The mineral surface area available for reaction is that which is exposed to gaseous and aqueous phase reactants. This excludes mineral surfaces that occur interstitial to or included within other nonporous minerals.

There are three major ways in which particle size variation can alter the magnitudes of exposed acid-producing and acid-neutralizing mineral surface areas and, consequently, the relative rates of acid production and neutralization. First, particle size reduction can affect mineral contents by preferential concentration of minerals in certain size fractions due to the hardness of the mineral relative to other minerals present in the rock. For example, softer minerals tend to concentrate in finer size fractions (Lapakko 1994). Second, as particle size decreases the specific surface area (surface area per unit mass) of particles increases. Third, as particle size decreases individual minerals tend to be released from the rock matrix, a phenomenon referred to as "mineral liberation" in the field of mineral processing. As a result of this liberation, all surfaces of a mineral grain are exposed for reaction. In contrast, the surfaces

of minerals present within larger rock particles will not have ready access to oxygen or interstitial water.

The effects of solid-phase changes introduced as a result of particle size reduction can be manifested in several aspects of drainage quality. These include drainage pH, the duration of the period of circumneutral drainage prior to drainage acidification (“lag time”), the fraction of acid-neutralizing minerals available to maintain pH in an environmentally acceptable range, and the relative rates of acid production and acid neutralization. The following text discusses the variation of these drainage quality aspects with particle size for three different rock types and provides insight on solid-phase factors that influence the variations.

### Norite

The major host rock minerals in the norite were plagioclase, olivine, hypersthene, and biotite (Table 1) with grain sizes on the order of two to ten millimeters, less than about 0.5 mm, less than 0.1 mm, and less than 0.5 mm, respectively. The AP(S<sub>T</sub>) values for the six size fractions ranged from 26 to 47 g CaCO<sub>3</sub> eq kg<sup>-1</sup>. AP(S<sub>T</sub>) of four of the fractions ranged from 26 to 29 g CaCO<sub>3</sub> eq kg<sup>-1</sup>, and was roughly 50 percent higher in the <0.053 and 0.149-0.5 mm fractions. NP[(Ca+Mg)CO<sub>3</sub>] ranged from <0.11 to 7.3 g CaCO<sub>3</sub> eq kg<sup>-1</sup> and tended to increase as particle size decreased (Table 2). Thus, particle size reduction resulted in some degree of preferential distribution of both sulfide and carbonate minerals.

Sulfide minerals identified were pyrrhotite, chalcopyrite, and cubanite, typically ranging from 50 to 500 μm. The rock chemistry indicated roughly 30 to 40 percent of the S was associated with pyrrhotite, 50 to 60 percent with chalcopyrite and cubanite, and about 10 percent with pentlandite, although this mineral was not detected in the mineralogical examination. The sulfide minerals occurred interstitial to and, less frequently, included in the relatively coarse-grained rock forming minerals. The degree of sulfide mineral surface exposure (fraction of total sulfide mineral surface area exposed) ranged from around six percent in the large particles to at least 98 percent in the fractions finer than two millimeters (Table 2).

Table 1. Approximate mode of minerals in the rock samples selected for testing<sup>1</sup>.

Rock	Rock Forming Minerals	Sulfide Minerals	Carbonate Minerals
norite	plagioclase (30-40) olivine (20-40) hypersthene (7-16) biotite (2-8)	pyrrhotite (1-9) chalcopyrite (tr <sup>2</sup> ) cubanite (tr)	calcite (tr)
diatreme	quartz (40-65) potassium feldspar (15-28) sericite (9-16)	pyrite (4-7)	siderite (4-8) rhodochrosite (2) kutnahorite (3)
mudstone	quartz (24-56) mica (23) potassium feldspar (13-37)	pyrite (5)	dolomite (7) siderite (1)

<sup>1</sup> Values in parentheses represent approximate modes in weight percent as determined by microprobe analysis. The mode was determined by point count of 100 grains using the microprobe. The percentage of sulfide and carbonate minerals does not necessarily coincide with those calculated based on chemistry due the low content and relatively small number of grains in the point count.

<sup>2</sup> tr = trace

Table 2. Acid-producing and acid-neutralizing characteristics of rocks.

Particle Size	S <sub>Total</sub>	S as SO <sub>4</sub>	CO <sub>2</sub>	AP(S <sub>T</sub> )	NP[(Ca+Mg)CO <sub>3</sub> ]	Sulfide Mineral Exposure	Carbonate Mineral Exposure
mm	percent			G CaCO <sub>3</sub> eq kg <sup>-1</sup>		percent	
Norite							
<0.053	1.51	0.08	0.32	47	7.3	100	100
0.053-0.149	0.87	0.08	0.10	27	2.3	100	78
0.149-0.5	1.29	0.09	0.06	40	1.4	100	36
0.5-2.0	0.88	0.07	0.05	28	1.1	98	11
2.0-6.35	0.83	0.06	0.09	26	2.1	23	1.6
6.35-19	0.93	0.03	<0.01	29	<0.11	5.9	0.4
Diatreme							
<0.053	0.95	0.16	0.96	30	5.9	100	100
0.053-0.149	1.98	0.04	1.32	62	8.1	100	100
0.149-0.5	2.34	0.03	1.60	73	9.8	100	100
0.5-2.0	1.9	0.05	1.73	59	11	67	100
2.0-6.35	1.5	0.04	1.46	47	9.0	12	26
Mudstone							
<0.053	2.83	0.28	0.88	88	20	100	100
0.053-0.149	3.01	0.08	1.64	94	37	100	100
0.149-0.5	2.61	0.07	1.68	82	38	100	100
0.5-2.0	2.79	0.11	1.40	87	32	67	82
2.0-6.35	3.52	0.13	1.27	110	29	12	15
6.35-19	3.46	0.14	1.89	108	43	3.0	4.0

Assuming all solid-phase carbon dioxide was present as calcite, the calcite content of all fractions was less than or equal to about 0.7 percent (Table 2). Only two calcite grains were observed during microprobe analysis and their diameters were 30 and 50  $\mu\text{m}$ . The calculated fraction of surface area exposed increased from less than one percent in the coarsest fraction and reached 100 percent only in the finest fraction (Table 2). Because the calcite exposure was based on observation of only two grains, these values must be interpreted with caution. Nonetheless, particle size reduction increased the fraction of mineral surface area exposed for both sulfide minerals and calcite. However, the fraction of mineral surface area exposed for sulfide minerals increased more rapidly than that for calcite (Table 2).

All size fractions of the norite ultimately yielded drainage pH values below 6.0. For finer size fractions pH tended to decrease through the initial 200 weeks then increase. For particle size fractions larger than 0.5 mm, drainage pH tended to decrease slowly throughout the experiment (Fig. 1). The lag time (time from the beginning of the experiment to the time drainage pH dropped below 6.0) and minimum pH increased with increasing particle size. The lag time for the four smallest particle size fractions ranged from 16 to 25 weeks, as opposed to 175 to 403 weeks for the two largest size fractions. For the 465-week period of record the

minimum pH ranged from 4.0 to 4.2 for the three finest fractions, from 4.8 to 4.9 for the 0.5-2.0 and 2.0-6.35 mm fractions, and the largest fraction produced a minimum pH of 5.8 (Fig. 1).

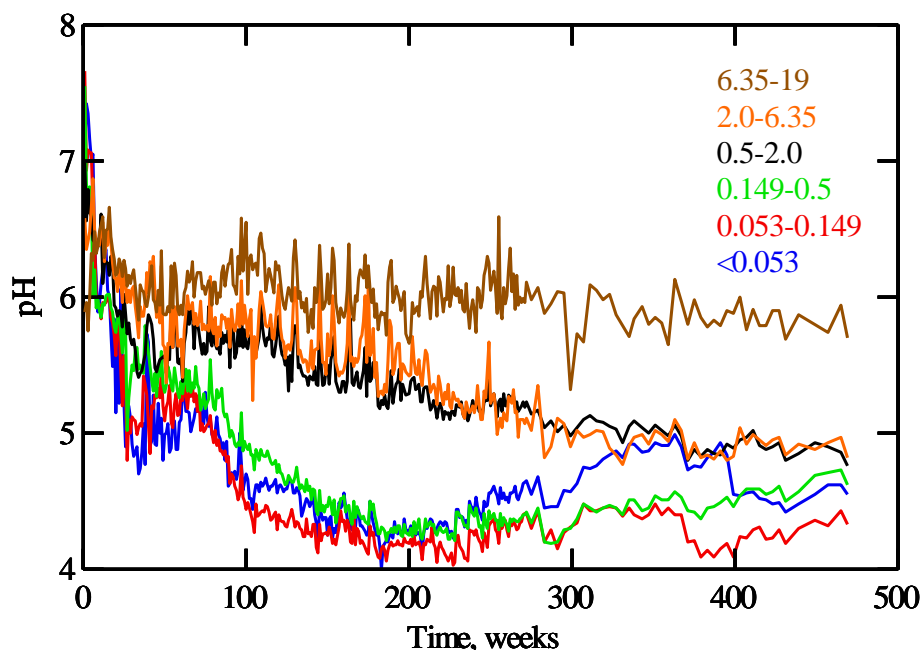


Figure 1. Drainage pH from the norite generally decreased as particle size (mm) decreased because pyrrhotite surface area increased to a greater degree than silicate mineral surface area.

The ENP values ranged from 0.4 to 2.8 g CaCO<sub>3</sub> eq kg<sup>-1</sup> and generally increased with decreasing particle size (Table 3). NP[(Ca+Mg)CO<sub>3</sub>] values also generally increased with decreasing particle size, and affected the ENP dependence on particle size to some degree. It should be noted that Mg release contributed roughly 50 to 60 percent of the ENP for all fractions except the <0.053 mm fraction, in which the Mg release accounted for 39 percent. This fraction had the highest calcite content, and calculations indicated all of the calcite was exposed, which could account for the higher Ca contribution to ENP. The fact that Mg release contributed to the ENP of all fractions indicates that Mg silicate mineral dissolution contributed to acid neutralization while pH remained above 6. It is also possible that calcium silicate mineral dissolution contributed to the ENP.

The NP[(Ca+Mg)CO<sub>3</sub>] was present as calcite and its depletion while pH remained ≥ 6.0 must be calculated based on the Ca fraction of ENP. This calculation indicates that for fractions finer than 6.35 mm only 16 to 32 percent of the calcite dissolved to maintain pH ≥ 6.0. The Ca fraction of the ENP for the <0.053 mm fraction, in which the calcite was totally exposed, represented only 23% of the calcite indicated present based on carbon dioxide content. At this fine grain size it seems likely that all calcite should have dissolved to maintain pH ≥ 6. However, it was not until week 219 that Ca release was adequate to account for dissolution of the NP[(Ca+Mg)CO<sub>3</sub>] present (7.3 g CaCO<sub>3</sub> eq kg<sup>-1</sup>, Table 2). At this time drainage pH had been below 5.0 for more than two years.

Table 3. Percent depletion of acid production potential (AP(S<sub>T</sub>)) and neutralization potential (NP[(Ca+Mg)CO<sub>3</sub>], listed as NP in table).

Particle Size	Period of record	Lag Time <sup>1</sup>	AP(S <sub>T</sub> )	NP	Percent Depletion <sup>2</sup>		AP(S <sub>T</sub> ) Depletion at Lag Time Week	ENP (Ca,Mg) <sup>3</sup>	ENP/ NP
					AP(S <sub>T</sub> )	NP			
mm	weeks		g CaCO <sub>3</sub> eq kg <sup>-1</sup>				g CaCO <sub>3</sub> eq kg <sup>-1</sup>		percent
Norite									
<0.053	465	23	47	7.3	80	270	3.2	2.8 (1.7, 1.1)	38
0.053-0.149	465	16	27	2.3	120	710	1.6	1.4 (0.70, 0.65)	61
0.149-0.5	465	16	40	1.4	59	1100	1.2	0.98 (0.45, 0.53)	71
0.5-2.0	465	25	28	1.1	22	440	0.44	0.41 (0.20, 0.20)	36
2.0-6.35	465	175	26	2.1	8.3	85	0.85	0.76 (0.33, 0.43)	38
6.35-19	465	403	29	<0.11	2.2	540	0.58	0.57 (0.26, 0.31)	540
Diatreme									
<0.053	465	>465	30	5.9	6.8	42	>2.0	>2.5 (1.5, 0.93)	>42
0.053-0.149	465	427	62	8.1	14	90	6.9	7.2 (2.9, 4.3)	89
0.149-0.5	465	485 <sup>4</sup>	73	9.8	7.2	81	7.2	7.9 (3.6, 4.3)	81
0.5-2.0	465	>465	59	11	5.5	74	>3.3	>7.8 (3.6, 4.2)	>71
2.0-6.35	465	427	47	9.0	10	54	4.4	4.7 (1.5, 3.2)	52
Mudstone									
<0.053	134	>134	88	20	4.3	54	>3.8	>11	>55
0.053-0.149	385	367	94	37	34	100	21	36 (20, 16)	97
0.149-0.5	465	449	92	38	32	100	23	36 (21, 15)	95
0.5-2.0	335	239	87	32	50	110	27	28 (16, 12)	88
2.0-6.35	134	0	110	29	32	82	0.17	0	0
6.35-19	134	0	108	43	13	22	0.11	0	0

<sup>1</sup>Number of weeks that the drainage pH remained consistently above 6.0.

<sup>2</sup>For the entire period of record.

<sup>3</sup>Values in parentheses represent the ENP associated with Ca and Mg, respectively.

<sup>4</sup>Drainage pH decreased below 6.0 at week.

This suggests that error may have been introduced into the calculation of NP[(Ca+Mg)CO<sub>3</sub>], perhaps in sample splitting for or analysis of the low solid-phase CO<sub>2</sub> contents on which this value was determined. Alternatively, error may have been introduced in estimating the extent of exposed calcite surface, which was calculated based on two calcite grains. Calcite grains as small as 30 microns were reported to be present and conceivably could have occurred interstitial to or included in larger particles in even the <0.053 mm fraction. Such occurrence would have limited their availability for reaction. Furthermore, it is likely that larger grains would be detected during microprobe analysis, but smaller grains may have been missed. White et al. (2005) reported calcite occurring in granitoid rocks as small (3-10 μm) disseminated grains and included in plagioclase. These occurrences would have been difficult to detect with the analytical approach used. These suggest that the degree of calcite exposure for this rock may

represent a maximum value. That is, a substantial fraction of the calcite may have occurred as fine grains included in other mineral grains or within rock particles and not exposed for reaction.

In contrast, the Ca fraction of the ENP for the 6.35-19 mm fraction was 2.4 times that present as calcite in the sample. Furthermore, the entire ENP was more than five times the NP[(Ca+Mg)CO<sub>3</sub>]. This, in conjunction with the fact that Mg contributed over half of the ENP, indicates that silicate mineral dissolution was responsible for most of the acid neutralization while drainage pH remained above 6. This is reasonable given the slow rate of SO<sub>4</sub><sup>-2</sup> release from this sample.

The NP[(Ca+Mg)CO<sub>3</sub>] depletions calculated over the duration of dissolution typically ranged from 270 to 1100 percent (Table 3). This indicates the total Ca and Mg release during the experiment exceeded that present in carbonate minerals. The excess Ca and Mg release was the result of plagioclase and Mg-bearing silicates present (Table 1).

Release rates of SO<sub>4</sub><sup>-2</sup>, Ca, and Mg generally increased as particle size decreased, but SO<sub>4</sub><sup>-2</sup> release rates increased to a greater degree than the sum of Ca and Mg release rates (Table 4). (It should be noted that the maximum Mg release rate occurred in the 0.149-0.5 mm fraction and was 25 percent higher than that for the finest fraction, and the reason for this is not known.) In the largest size fraction, the sum of Ca and Mg release rates was more than 90 percent of the SO<sub>4</sub><sup>-2</sup> release rate. This fraction decreased to 50 percent as particle size decreased (Table 4). This indicates that the fraction of acid neutralized decreased with decreasing particle size, which is consistent with the pH dependence on particle size. Furthermore, the observed rates and pH dependence are consistent with the pyrrhotite surface area increasing to a greater degree than the neutralizing mineral surface area as particle size decreased. The high S contents of the <0.053 and 0.149-0.5 mm fractions (Table 2) would contribute to a preferential increase in pyrrhotite surface area. However, S content of fractions coarser than 0.053 mm varied from 0.83 to 0.93 percent, a fairly small range. Nonetheless, the ratio of the sum of Ca and Mg release rates to SO<sub>4</sub><sup>-2</sup> rate decreased steadily with decreasing particle size (Table 4). The degree of sulfide mineral exposure correlated with this trend, as well as the trends observed for drainage pH and lag time. In all but the finest fraction, rates of Mg release exceeded those of Ca release, indicating that over the duration of the experiment, Mg release from silicate mineral dissolution contributed to acid neutralization.

In summary, acid production by the norite increased with decreasing particle size. Consequently as particle size decreased, drainage pH values, lag times, and the ratio of neutralizing mineral dissolution rates to acid producing mineral oxidation rates decreased. These three drainage quality descriptors correlated well with the degree of sulfide mineral exposure. This indicates clearly that particle size reduction preferentially increased the acid-producing mineral surface area to a greater extent than the acid-neutralizing mineral surface area. The fraction of NP[(Ca+Mg)CO<sub>3</sub>] dissolved to maintain pH ≥ 6.0 was not a reliable indicator of neutralizing mineral availability because acid neutralization by silicate minerals during this time typically equaled or exceeded that by calcite. Silicate mineral dissolution clearly contributed a substantial amount of the acid neutralization for periods after pH decreased below 6.0, as indicated by Ca and Mg release over the course of the experiment that was typically at least 270 percent of the NP[(Ca+Mg)CO<sub>3</sub>] by (Table 3).

Table 4. Average sulfate, calcium, and magnesium release rates.

Particle Size	Period of Record	Lag Time <sup>1</sup>	AP(S <sub>T</sub> )	NP[(Ca+Mg)CO <sub>3</sub> ]	Average Release Rates <sup>2</sup>			
					SO <sub>4</sub>	Ca	Mg	(Ca+Mg)/SO <sub>4</sub>
mm	weeks		g CaCO <sub>3</sub> eq kg <sup>-1</sup>		mmol (kg≅ wk) <sup>11</sup>			
Norite								
<0.053	465	23	47	7.3	0.802	0.244	0.165	0.51
0.053-0.149	465	16	27	2.3	0.697	0.167	0.177	0.49
0.149-0.5	465	16	40	1.4	0.508	0.102	0.207	0.61
0.5-2.0	465	25	28	1.1	0.131	0.033	0.073	0.81
2.0-6.35	465	175	26	2.1	0.046	0.015	0.023	0.83
6.35-19	465	403	29	<0.11	0.014	0.006	0.007	0.93
Diatreme								
<0.053	465	465	30	5.9	0.041	0.031	0.020	1.24
0.053-0.149	465	427	62	8.1	0.181	0.062	0.093	0.86
0.149-0.5	465	485 <sup>3</sup>	73	9.8	0.099	0.076	0.092	1.70
0.5-2.0	465	465	59	11	0.070	0.078	0.089	2.39
2.0-6.35	465	427	47	9.0	0.101	0.033	0.072	1.04
Mudstone								
<0.053	134	134	88	20	0.215	0.405	0.312	3.34
0.053-0.149	385	367	94	37	0.766	0.550	0.416	1.26
0.149-0.5	465	449	92	38	0.467	0.467	0.343	1.73
0.5-2.0	335	239	87	32	1.298	0.572	0.423	0.77
2.0-6.35	134	0	110	29	2.640	0.959	0.815	0.67
6.35-19	134	0	108	43	1.057	0.350	0.357	0.67

<sup>1</sup> Number of weeks drainage pH remained consistently above 6.0.

<sup>2</sup> For weeks three to the end of the period of record (excluding initial release from weeks 0-2).

<sup>3</sup> Drainage pH decreased below 6.0 at week 485 and rates of release calculations end at week 465.

### Diatreme

The major rock forming minerals in the diatreme were quartz, potassium feldspar, and muscovite (Table 1). AP(S<sub>T</sub>) in the five size fractions ranged from 30 to 73 g CaCO<sub>3</sub> eq kg<sup>-1</sup> and NP [(Ca+Mg)CO<sub>3</sub>] from 5.9 to 11 g CaCO<sub>3</sub> eq kg<sup>-1</sup> (Table 2). The AP(S<sub>T</sub>) ranged from roughly 50 to 70 g CaCO<sub>3</sub> eq kg<sup>-1</sup> for the four largest fractions and was half as large in the finest fraction. NP [(Ca+Mg)CO<sub>3</sub>] ranged from approximately 8 to 11 g CaCO<sub>3</sub> eq kg<sup>-1</sup> in the four larger fractions and was about 60 percent as large in the finest fraction. Thus, both AP(S<sub>T</sub>) and NP [(Ca+Mg)CO<sub>3</sub>] tended to be low in the finest size fraction. Pyrite, manganese-rich siderite

( $\text{Fe}_{1.50}\text{Mn}_{0.23}\text{Ca}_{0.14}\text{Mg}_{0.12}(\text{CO}_3)_2$ ), rhodochrosite ( $\text{Mn}_{0.96}\text{Fe}_{0.77}\text{Mg}_{0.15}\text{Ca}_{0.14}(\text{CO}_3)_2$ ), and ferroan kutnahorite ( $\text{Mn}_{0.89}\text{Ca}_{0.51}\text{Fe}_{0.42}\text{Mg}_{0.18}(\text{CO}_3)_2$ ) were detected and analyzed by microprobe.

The initial mineralogical analysis indicated coarse and fine-grained sulfide minerals occurred as both disseminated grains and in veinlets. Subsequent microprobe analysis confirmed the presence of disseminated sulfide and carbonate minerals occurring as both coarse and fine grains (Fig. 2). The observed sulfide grain sizes ranged from about 100 to over 500  $\mu\text{m}$  and the carbonate grains varied from less than 100 to as large as 1000  $\mu\text{m}$ . The extent of sulfide mineral surface exposure ranged from 12 percent in the 2.0-6.35 mm fraction to 100 percent in fractions finer than 0.5 mm. Carbonate mineral surface areas were entirely exposed in all fractions finer than 2.0 mm (Table 2).

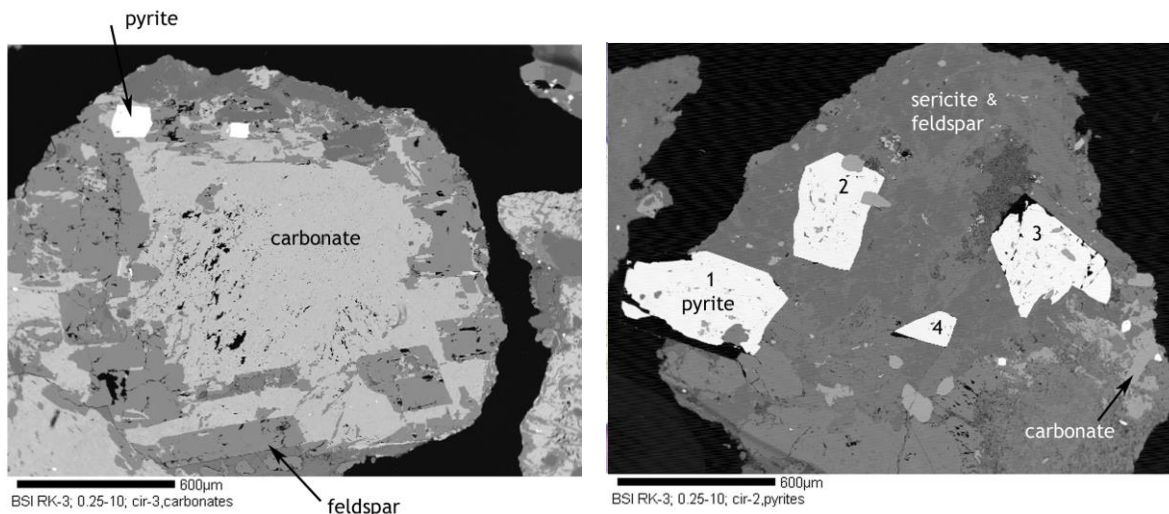


Figure 2. For the diatreme, disseminated sulfide and carbonate minerals occur as both coarse and fine grains as can be seen in these two backscatter photomicrographs.

Drainage pH from all samples decreased with time and three of the five particle size fractions produced some acidic drainage (Fig. 3). The <0.053 mm sample did not readily transmit flow probably due to the sericite content, which was roughly 10 percent. The  $\text{AP}(\text{S}_T)$  and  $\text{NP}[(\text{Ca}+\text{Mg})\text{CO}_3]$  depletion (Table 3) and rates of release (Table 4) for the sample were anomalously low considering the particle size. The low conductivity of the sample most likely limited reaction product transport from the sample. Furthermore, it may have limited oxygen transport to sulfide mineral surfaces and, consequently, sulfide mineral oxidation. These limitations were not conducive to assessing the oxidative dissolution behavior of the samples. The results must be interpreted with caution. The 0.053-0.149, 0.149-0.5 and 2.0-6.35 mm particle size fractions produced pH values less than 6.0 after 415, 485, and 403 weeks, respectively. The period of record chosen for presentation was 465 weeks. After this period was selected, the 0.149-0.5 mm fraction acidified and the information was subsequently included to provide an additional data point. The <0.053 and 0.5-2.0 mm fractions did not produce acidic drainage, although after 465 weeks of reaction drainage pH values were decreasing and near 6.0 (Fig. 3).

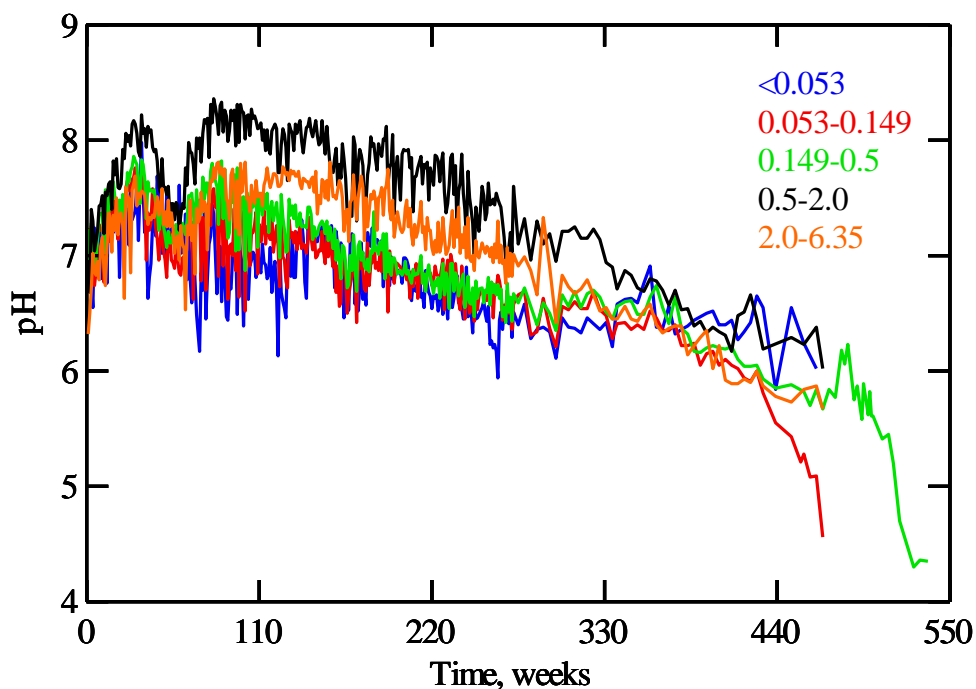


Figure 3. Drainage pH for the diatreme was not strongly dependent on particle size (mm; including 536 weeks for the 0.149-0.5 mm size fraction). Sulfide and carbonate mineral occurrences were similar and, consequently, their available surface areas were affected similarly by particle size reduction.

At the time of drainage acidification the respective ENP values for the 0.053-0.149, 0.149-0.5, and 0.5-2.0 mm fractions were 7.2, 7.9, and 4.7 g  $\text{CaCO}_3$  eq  $\text{kg}^{-1}$  (Table 3). As mentioned previously, the  $\text{NP}[(\text{Ca}+\text{Mg})\text{CO}_3]$  varied with particle size, and the ENP values represented 89, 82, and 52 percent of the respective  $\text{NP}[(\text{Ca}+\text{Mg})\text{CO}_3]$  (Table 3). Thus, the fraction of  $\text{NP}[(\text{Ca}+\text{Mg})\text{CO}_3]$  that reacted to neutralize acid and maintain drainage pH  $\geq 6.0$  decreased as particle size increased. The Ca and  $\text{MgCO}_3$  minerals present in the finer fractions were apparently more readily available for reaction than those in the larger particles. For these three samples, Ca release contributed 32 to 46 percent of the ENP. This is somewhat less than would be expected based on stoichiometric dissolution of the carbonates present. It is possible that dissolution of the sericite, which did contain a small amount of Mg, contributed some of the Mg released while pH exceeded 6.0. The fractions of initial  $\text{NP}[(\text{Ca}+\text{Mg})\text{CO}_3]$  depleted from the <0.053 and 0.5-2.0 mm fractions after 465 weeks were 42 and 71 percent, respectively. The drainage pH from these fractions had not decreased below 6.0 at this time. As noted above, flow through the <0.053 mm size fraction was inhibited and most likely limited the  $\text{NP}[(\text{Ca}+\text{Mg})\text{CO}_3]$  depletion.

The 0.053-0.149 mm fraction produced the highest average  $\text{SO}_4^{-2}$  release rate, followed by the 2.0-6.35 and 0.149-0.5 mm fractions, for which rates were essentially equal (Table 4). These

three samples also produced the lowest pH values. When normalized for S content,  $\text{SO}_4^{2-}$  release rates for the <0.053, 0.149-0.5, and 0.5-2.0 mm fractions were similar. The rates for the 2.0-6.35 and 0.053-0.149 mm fractions were higher by factors of 1.7 and 2.5, respectively. For all size fractions, less than 20 percent of the S initially present was released to drainage during the course of the experiment. The  $\text{SO}_4^{2-}$  release rates from the <0.053 mm fraction decreased by more than an order of magnitude after week 135 (from 1.036 to 0.027  $\mu\text{mol/g/wk}$ ), producing the lowest rates observed for all particle size fractions of the diatreme. As discussed previously, physical factors may have reduced the reaction product transport and possibly of oxygen transport to the sulfide mineral surfaces at this time.

In summary drainage pH values from all diatreme size fractions decreased slowly over time and there was not a strong dependence on particle size. Similarly, variations in particle size did not greatly influence lag time or the ratio of neutralizing mineral dissolution rates to acid producing mineral oxidation rates. These observations indicate that the reduction did not appear to greatly affect the relative surface areas of acid-producing and acid-neutralizing minerals available for reaction. For the three size fractions that produced drainage pH values below 6.0, the fraction of  $\text{NP}[(\text{Ca}+\text{Mg})\text{CO}_3]$  that dissolved to maintain pH greater than 6.0 increased with decreasing particle size. This indicated that the carbonate mineral surface area available for reaction increased with decreasing particle size, and this is consistent with the increasing specific surface area with decreasing particle size and the reported degree of carbonate mineral exposure estimated by microprobe analysis. Because sulfide mineral surface areas also increased with decreasing particle size, the ratio of acid-producing to acid-neutralizing mineral surface areas available for reaction did not vary greatly with particle size.

### Mudstone

The major rock forming minerals in the mudstone were quartz, mica, and potassium feldspar (Table 1).  $\text{AP}(\text{S}_\text{T})$  for the six particle size fractions ranged from 82 to 110 g  $\text{CaCO}_3$  eq  $\text{kg}^{-1}$ . Values were near 110 g  $\text{CaCO}_3$  eq  $\text{kg}^{-1}$  for the two largest size fractions and ranged from 82 to 94 g  $\text{CaCO}_3$  eq  $\text{kg}^{-1}$  for the four smaller size fractions.  $\text{NP}[(\text{Ca}+\text{Mg})\text{CO}_3]$  ranged from 20 to 43 g  $\text{CaCO}_3$  eq  $\text{kg}^{-1}$  and showed no systematic variation with particle size (Table 2). The presence of pyrite was confirmed by microprobe analysis, as was the presence of dolomite ( $\text{Ca}_{1.06}\text{Mg}_{0.83}\text{Fe}_{0.06}\text{Mn}_{0.05}(\text{CO}_3)_2$ ) and a small amount of siderite ( $\text{Fe}_{1.80}\text{Mg}_{0.18}\text{Mn}_{0.02}(\text{CO}_3)_2$ ).

The initial mineralogical analysis indicated the pyrite occurred with quartz in veinlets that were “relatively open and porous”. This suggests that in larger rock particles, the pyrite would be accessible to air and water, and therefore available for oxidation. Subsequent microprobe analysis indicated that pyrite occurred in four different textural settings, which were, in order of decreasing abundance: (1) one half- to several-millimeter size agglomerates of anhedral and subhedral pyrite grains on the order of 40  $\mu\text{m}$  in diameter, intergrown with the silicate minerals, that accounted for the majority of the pyrite in the sample; (2) isolated, euhedral grains roughly 50 to 450  $\mu\text{m}$  in diameter; (3) in 20-200  $\mu\text{m}$  - wide veins, both intergrown with other phases, such as potassium feldspar, and as the only phase in the vein; and (4) as framboids (5 to 95  $\mu\text{m}$ ) (Fig. 4). The aggregates referred to in (1) consisted of pyrite grains on the order of 40  $\mu\text{m}$  in diameter (Fig. 4A) and may be the “relatively open and porous” veinlets referred to in the initial mineralogical analysis. The estimated fraction of pyrite surface exposed ranged from 12 percent

in the largest particle size fraction to 100 percent for the three fractions finer than 0.5 mm (Table 2).

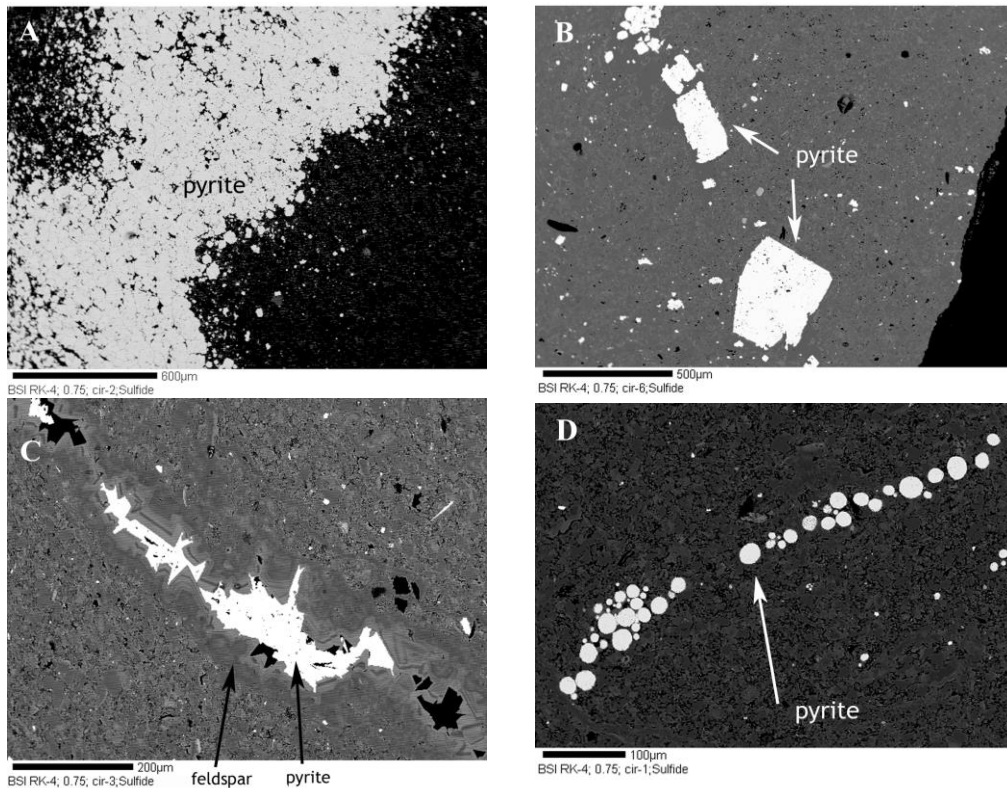


Figure 4. Backscatter microprobe images of unleached sample of the >19 mm size fraction of the mudstone in thin section. Pyrite occurs as (A) massive agglomerations of grains (dark material to lower right is epoxy), (B) isolated euhedral grains, (C) in veins with other minerals, and (D) framboidal grains.

Carbonates and carbonate minerals also occurred with quartz in veinlets that were described as “tight” in the initial mineralogical examination. This occurrence would tend to limit carbonate mineral reactivity in larger rock particles by limiting the surface area available to acidic drainage. Microprobe examination revealed massive (d ~ 200 µm) dolomite intergrown with quartz, feldspar, and sericite and dolomite intergrown with potassium feldspar in a vein about 200 by 800 µm. Thus the carbonate grains were considerably larger than the pyrite grains. Mineralogical assessment indicated the degree of carbonate mineral liberation increased from four percent in the 6.35-19 mm fraction to 100 percent in the 0.149-0.5 mm fraction (Table 2).

All size fractions except the <0.053 mm fraction ultimately yielded acidic drainage pH values. The <0.053 mm sample did not readily transmit flow, likely due to the presence of approximately 20 percent mica, and was terminated after 134 weeks of dissolution. In general, this sample was less reactive than the others, most likely due to factors similar to those discussed for the <0.053 mm fraction of the diatreme. The minimum pH values for the remaining five size

fractions were all below 3.0, and comparison among the minimum values must consider the durations of testing and the remnant dolomite content, as well as particle size factors (Fig. 5).

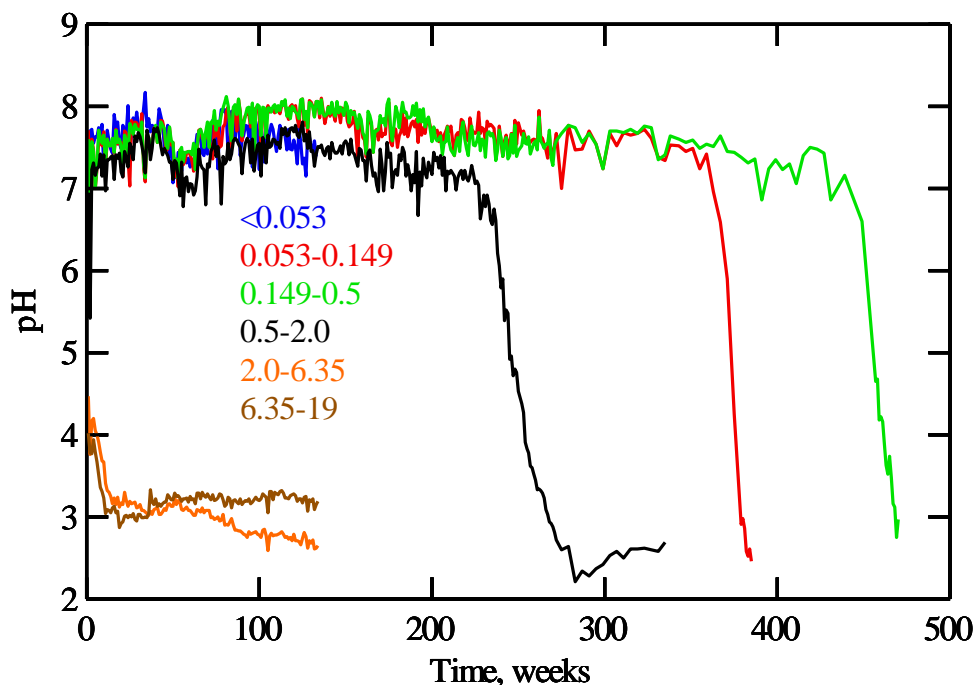


Figure 5. Drainage pH versus time for the mudstone particle size fractions (in mm). Lag time tended to increase as particle size decreased due to increasing dolomite surface area with decreasing particle size.

The pH of drainage from the two largest particle size fractions of the mudstone was continuously below 6.0, despite  $\text{NP}[(\text{Ca}+\text{Mg})\text{CO}_3]$  values of roughly 30 to 40  $\text{g CaCO}_3 \text{ eq kg}^{-1}$ . Because drainage pH never exceeded 6.0 the ENP for these samples was zero. The dolomite present was dissolving, as indicated by the Ca and Mg release, but the rate of dissolution was too slow to neutralize all of the acid produced by Fe sulfide oxidation. This suggests that the dolomite surface area available for reaction was limited by the extent of dolomite exposure, which was estimated as 4 to 15 percent of the large grains in these fractions (Table 2). The estimated extent of pyrite exposure was similarly low but clearly did not inhibit acid production, which is particularly surprising given the large particle size of the rocks. This indicates that the pyrite surface area exposed was not a controlling factor in the rate of acid production. This peculiarity is discussed below in the context of rates of release. These two reactors were terminated after 135 weeks.

In contrast, the 0.5-2.0, 0.149-0.5, and 0.053-0.149 mm size fractions produced acidic drainage after respective lag times of 239, 449, and 367 weeks (Fig. 5), yielding ENP values of 27 to 36  $\text{g CaCO}_3 \text{ eq kg}^{-1}$ . Thus, the fractions of  $\text{NP}[(\text{Ca}+\text{Mg})\text{CO}_3]$  available for maintaining drainage  $\text{pH} \geq 6.0$  ranged from zero for the two largest size fractions to 88, 95, and 97 percent

for the three finer fractions (Table 3). These values are in good agreement with carbonate depletion calculated from analysis of the solids after dissolution testing. From largest to smallest particle size fractions, these values were 22, 91, 100, 100, and 100 percent. (Solid phase analysis indicated 78 percent depletion of carbonates in the <0.053-mm fraction in which flow was inhibited, and this was substantially different than the 54 percent depletion calculated based on drainage quality.) These available NP[(Ca+Mg)CO<sub>3</sub>] values agree reasonably well with the increasing carbonate mineral specific surface area and extent of surface exposure with decreasing particle size reported for this rock (Table 2). Furthermore, particle size reduction would increase the specific surface area of the exposed carbonates, thus increasing rates of reaction per unit mass carbonate mineral. Thus, the specific surface area and availability of NP[(Ca+Mg)CO<sub>3</sub>] increased as particle size decreased, as suggested by the initial description of the carbonate grain size, mineral mode of occurrence and the subsequent quantification of the degree of carbonate mineral liberation. Similarly, this suggests the exposed dolomite (and to a lesser extent, siderite) surface area increased as particle size decreased.

For periods when pH exceeded 6.0, the rate of Ca release averaged 1.34 times that of Mg release. This compares well with the Ca to Mg ratio of 1.28 in the dolomite. The close agreement indicates that dolomite dissolution was largely responsible for acid neutralization to maintain pH ≥ 6.0 and lends further credence to the calculations of the fraction of dolomite depleted.

The average SO<sub>4</sub><sup>-2</sup> release rates from the three largest size fractions were 1.4 to 5.7 times the rates for the 0.053-0.149 and 0.149-0.5 mm fractions (Table 4). (The flow problems encountered in the finest fractions make rate comparisons with other fractions tenuous.) This suggests that the pyrite surface area available in the largest fractions was greater than that in the finer fractions, and this runs counter to reason. Additional data analysis was conducted to further assess the variation of SO<sub>4</sub><sup>-2</sup> release with particle size.

Comparison of SO<sub>4</sub><sup>-2</sup> release rates from the mudstone (Table 4) is compromised because pyrite content varied among size fractions and the periods of record for rate calculations varied. To account for these variables, rates of SO<sub>4</sub><sup>-2</sup> release per gram pyrite were determined for the period prior to week 134. The resultant rates for the three largest fractions were 1.3 to 3.5 times those for the two finer fractions. If the exposed pyrite surface area were proportional to the inverse of mean rock particle diameter (as is the case for geometrically determined surface area) and the degree of mineral liberation, the pyrite surface areas for the three largest particle size fractions would be 0.02 to 17 percent of those of the two finer fractions. That is, the refined calculations also indicated that exposed pyrite surface area determined by this calculation had no influence on the rate of SO<sub>4</sub><sup>-2</sup> release.

The preceding analysis suggests that the methods of assessing exposed pyrite surface area were in error or that the rates of pyrite oxidation varied among particle size fractions. Pyrite oxidation rates are expressed relative to surface area (e.g. Williamson and Rimstidt 1994). Consequently, assuming the mechanism of pyrite oxidation is the same in all size fractions, the observed rates suggest the pyrite surface area exposed in the larger size fractions exceeds that in the finer fractions. The conditions under which this would occur are not apparent, but it is conceivable that there was not a large difference in pyrite surface area among size fractions. The predominant occurrence of pyrite was as agglomerates of anhedral and subhedral pyrite grains on the order of 40 μm in diameter. If these agglomerates occurred largely on the surface of the

larger particles, due to preferential fracturing of rock particles along these agglomerates, the majority of pyrite surface area present in the larger particle would be exposed. This would limit the magnitude of the difference in available pyrite surface area between the larger and smaller particles, particularly if there were some porosity among the individual pyrite grains. Because individual size fractions were not examined and porosity of the agglomerates was not determined, the likelihood of this concept was not assessed.

It is highly likely that the mechanism of oxidation for the two largest size fractions was different than that for the 0.053-0.149 and 0.149-0.5 mm fractions. Drainage from the two largest fractions was acidic immediately. Drainage pH values decreased below 4.0 at week 2 and were in the range of 3.0-3.5 by week 11. This suggests that the pyrite mineral surfaces had become acidic prior to inception of the dissolution test. The acidic conditions likely contributed to bacterial mediation of the sulfide mineral oxidation, thereby accelerating the oxidation rate. It is conceivable that acidic microenvironments in the 0.5-2.0 mm fraction were also conducive to bacterial catalysis. The lag time, 239 weeks, for this size fraction was the shortest of the finer samples. The 0.053-0.149 and 0.149-0.5 mm fractions produced circumneutral drainage for extended periods prior to acidification. Sulfate release rates after acidification increased by respective factors of 12 and 6 relative to those immediately prior to acidification, presumably due to microbial mediation of pyrite oxidation. This indicates that the acidic conditions associated with the larger particles were conducive to accelerating pyrite oxidation by roughly an order of magnitude. This most likely contributed to the elevated  $\text{SO}_4^{-2}$  release rates from the larger particle size fractions.

In the smaller particle size fractions, a greater extent of the carbonate mineral surface area was exposed and available for reaction (Table 2). Consequently, the carbonate minerals present in the finer fractions dissolved fast enough to neutralize the acid produced by the Fe sulfide mineral oxidation. Furthermore, with the more intimate contact of sulfide and carbonate mineral contact and elevated moisture content, acid is more likely to be neutralized before acidic microenvironments develop to a great extent. This in turn would inhibit bacterial acceleration of oxidation rates. Elevating the pH near sulfide minerals also enhances the precipitation of Fe oxyhydroxides on the sulfide mineral surfaces, thereby inhibiting the rate of oxidation.

In summary the lag time, the fraction of  $\text{NP}[(\text{Ca}+\text{Mg})\text{CO}_3]$  dissolved to maintain  $\text{pH} \geq 6.0$ , and the ratio of rates of acid neutralization (as indicated by the sum of Ca and Mg release rates) to acid production (as indicated by  $\text{SO}_4^{-2}$  release rate) all increased as particle size decreased. These three drainage quality descriptors indicate the dolomite surface area available for reaction increased as particle size decreased. The increased availability was reflected by the increased carbonate mineral exposure determined by mineralogic analysis and increasing dolomite specific surface area with decreasing particle size. Rates of  $\text{SO}_4^{-2}$  release tended to decrease with decreasing particle size, and it seems highly unlikely that this was due to decreasing available sulfide mineral surface area with decreasing particle size. This trend was apparently due to acidic conditions at the sulfide mineral surfaces of the large particles that were conducive to bacterial catalysis. That is, the pyrite oxidation rates (per unit surface area) for the acidic larger particles were greater than those in the circumneutral pH environment present in the finer particle size fractions. Exposure of a large percentage of the pyrite agglomerates on the large particle surfaces may have also contributed to the elevated  $\text{SO}_4^{-2}$  release from this fraction.

## **Conclusions**

The effects of rock particle size on drainage pH, lag time, fraction of NP[(Ca+Mg)CO<sub>3</sub>] available to maintain drainage pH  $\geq 6.0$ , and relative rates of acid production and acid neutralization were dependent on lithology. The dependence of these drainage quality predictors on particle size was due to the influence of particle size reduction on the relative abundance of exposed acid-producing and acid-neutralizing mineral surface areas. Mineralogical analysis of the solids provided insight into this influence.

As particle size of the low-carbonate norite decreased, drainage pH values, lag times, and the ratio of neutralizing mineral dissolution rates to acid producing mineral oxidation rates decreased. These three drainage quality descriptors correlated well with the degree of mineral exposure. This clearly indicates that particle size reduction preferentially increased the acid-producing mineral surface area to a greater extent than the acid-neutralizing mineral surface area.

The opposite particle size dependence was observed for the adularized mudstone containing an equivalent of two to four percent calcite. For the mudstone, the lag time, the fraction of NP[(Ca+Mg)CO<sub>3</sub>] dissolved to maintain pH  $\geq 6.0$ , and the ratio of rates of acid neutralization to acid production all increased as particle size decreased. These three drainage quality descriptors indicate the dolomite surface area available for reaction increased as particle size decreased. The increased availability was reflected by the increased carbonate mineral exposure determined by mineralogical analysis and increasing dolomite specific surface area with decreasing particle size. In contrast, SO<sub>4</sub><sup>-2</sup> release indicated pyrite oxidation was most rapid in the largest particle size fractions. Acidic conditions in these fractions developed prior to dissolution testing and most likely contributed to acceleration of pyrite oxidation by microbial mediation.

Drainage pH from the diatreme rock containing an equivalent of about one percent calcite, exhibited no strong dependence on particle size. Similarly, variations in particle size did not greatly influence lag time or the ratio of neutralizing mineral dissolution rates to acid producing mineral oxidation rates. These observations indicate that the reduction did not appear to greatly affect the relative surface areas of acid-producing and acid-neutralizing minerals. The NP[(Ca+Mg)CO<sub>3</sub>] that dissolved to maintain pH  $\geq 6.0$  was qualitatively indicated by optical microscope examination and semiquantitatively determined by microprobe estimations of carbonate mineral exposure.

The mineralogical methods used did not assess preferential breakage or potential porosity among agglomerated pyrite grains. Examining individual particle size fractions (rather than only the largest particle size as was done in this study) to determine if rock particles break preferentially along sulfide or carbonate veins would yield a better understanding of the mineral surface area exposed for reaction. Examination of grain mounts and thin sections using secondary electron imaging would better assess potential porosity in mineral agglomerates, an occurrence that was observed for pyrite in the mudstone.

## **Acknowledgments**

Funding for the current project was provided by the US Army Corps of Engineers RAMS program (DACW45-02-P-0205). Previous funding was supplied by the US Environmental Protection Agency (USEPA) under Agreement #CX-816270-01-0 and administered by the

Western Governors' Association (WGA), and subsequently under USEPA Grant Number X-8200322-01-0. Additional funding was supplied by the Minnesota Department of Natural Resources (MNDNR). Laboratory dissolution experiments were conducted by Kate Willis, Anne Jagunich, Cal Jokela, and Pat Geiselman. Anne Jagunich and Andrea Johnson were largely responsible for data management. Sharon Diehl of the U.S. Geological Survey and William White III of the US Bureau of Land Management diligently reviewed the draft paper and provided numerous comments that improved the content and clarity final submittal.

### Literature Cited

- American Public Health Association (APHA), American Water Works Association, Water Environment Federation. 1992. Standard methods for the examination of water and wastewater, 18th ed. American Public Health Association, Washington, D.C.
- Busenberg, E., Clemency, C.V. 1976. The dissolution kinetics of feldspars at 25 °C and 1 atmosphere CO<sub>2</sub> partial pressure. *Geochim. Cosmochim. Acta*, v. 40. p. 41-49. [http://dx.doi.org/10.1016/0016-7037\(76\)90192-7](http://dx.doi.org/10.1016/0016-7037(76)90192-7).
- Busenberg, E., Plummer, L.N. 1982. The kinetics of dissolution of dolomite in CO<sub>2</sub>-H<sub>2</sub>O systems at 1.5° to 65 °C and 0 to 1 atm PCO<sub>2</sub>. *American Journal of Science*, v. 282. p. 45-78. <http://dx.doi.org/10.2475/ajs.282.1.45>.
- Busenberg, E., Plummer, L.N. 1986. A comparative study of the dissolution and crystal growth kinetics of calcite and aragonite. *U.S. Geol. Surv. Bull.* 1578. p. 139-168.
- Chou, L., Garrels, R.M., Wollast, R. 1989. Comparative study of the kinetics and mechanisms of dissolution of carbonate minerals. *Chemical Geology*, v. 78, no. 3-4. p. 269-282. [http://dx.doi.org/10.1016/0009-2541\(89\)90063-62](http://dx.doi.org/10.1016/0009-2541(89)90063-62).
- Drever, J.I. 1988. *The geochemistry of natural waters*. Prentice Hall, Englewood Cliffs, New Jersey, 437 p.
- Greenberg, J., Tomson, M. 1992. Precipitation and dissolution kinetics and equilibria of aqueous ferrous carbonate vs. temperature. *Applied Geochemistry*, v. 7, no. 2. p. 185-190. [http://dx.doi.org/10.1016/0883-2927\(92\)90036-3](http://dx.doi.org/10.1016/0883-2927(92)90036-3).
- Hem, J.D. 1970. Study and interpretation of the chemical characteristics of natural water. *Geological Survey Water-Supply Paper* 1473, Washington, D.C., 363 p.
- Jambor, J.L. 1994. Mineralogy of sulfide-rich tailings and their oxidation products. p. 59-102. *In* *Environmental Geochemistry of Sulfide Mine-Wastes*. Mineralogical Association of Canada, Short Course Handbook, vol. 22.
- Kleinmann, R. L. P., Crerar, D. A., Pacelli, R. R. 1981. Biogeochemistry of acid mine drainage and a method to control acid formation. *Mining Eng.*, v. 33. p. 300-306.
- Kwong, Y.T.J., Ferguson, K.D. 1990. Water chemistry and mineralogy at Mt. Washington: Implications to acid generation and metal leaching. p. 217-230. *In* *Acid Mine Drainage: Designing for Closure*. (J.W. Gadsby, J.A. Malick & S.J. Day, eds). Bitech Publishers, Vancouver, British Columbia.

- Lapakko, K.L. 1990. Solid phase characterization in conjunction with dissolution experiments for prediction of drainage quality. p. 81-86. *In Proc. Western Regional Symposium on Mining and Mineral Processing Wastes*, F. Doyle (ed.), Soc. for Mining, Metallurgy, and Exploration, Inc., Littleton, CO.
- Lapakko, K.L. 1994. Comparison of Duluth Complex rock dissolution in the laboratory and field. p. 419-428. *In Proc. Third International Conference on the Abatement of Acidic Drainage* (April 25-29, 1994, Pittsburgh, PA). Vol 1.  
<https://doi.org/10.21000/JASMR94010419>
- Lapakko, K.L., Antonson, D.A. 1994. Oxidation of sulfide minerals present in Duluth Complex rock: A laboratory study. p. 593-607. *In Environmental Geochemistry of Sulfide Oxidation*; ACS Symposium Series 550 (August 23-28, 1992). American Chemical Society, Washington, D.C.
- Lapakko, K.A., Antonson, D.A. 2002. Drainage pH, acid production, and acid neutralization for Archean greenstone rock. Preprint 02-73. *In Proc. 2002 SME Annual Meeting* (Phoenix, AZ, February 25-27). Soc. For Mining, Metallurgy, and Exploration, Inc. Littleton, CO.
- Lapakko, K.L., Antonson, D.A., Wagner, J.R. 1997. Mixing of limestone with finely crushed acid-producing rock. p. 1345-1360. *In Proc. Fourth Intl. Conf on Acid Rock Drainage*, Vol. 3 (Vancouver, British Columbia, Canada, May 31 - June 6, 1997).
- Lapakko, K.L., Engstrom, J.N., Antonson, D.A. 2004. Long Term Dissolution Testing of Mine Waste. Report the US Army Corps of Engineers Contract/Order No. DACW45-02-P-0205. Division of Lands and Minerals, MN DNR, St. Paul, MN. 154 p. plus appendices.
- Nelson, M.B. 1978. Kinetics and mechanisms of the oxidation of ferrous sulfide. Ph.D. Thesis, Stanford University, Palo Alto, CA. 286 p.
- Nesbitt, H.W., Jambor, J.L. 1998. Role of mafic minerals in neutralizing ARD, demonstrated using a chemical weathering methodology. p. 403-421. *In Cabri, L.J. and Vaughan, D.J. (eds.), Modern Approaches to Ore and Environmental Mineralogy. Mineralogical Association of Canada Short Course Series, vol. 27.*
- Nordstrom, D.K. 1982. Aqueous pyrite oxidation and the consequent formation of secondary iron minerals. p. 37-56. *In Acid Sulfate Weathering*. J.A. Kittrick, D.S. Fanning, and L.R. Hossner (eds.), Soil Sci. Soc. America Spec. Pub. 10.
- Nordstrom, D.K. 1999. Some fundamentals of aqueous geochemistry. p. 117-123. *In The Environmental Geochemistry of Mineral Deposits. Part A: Processes, Techniques, and Health Issues*, vol. 6A, chapter 4. *Reviews in Economic Geology*. Society of Economic Geologists, Inc., Chelsea, MI.
- Nordstrom, D.K., Alpers, C.N. 1999. Geochemistry of acid mine waters. p. 133-160. *In The Environmental Geochemistry of Mineral Deposits. Part A: Processes, Techniques, and Health Issues*, vol. 6A, chapter 4. *Reviews in Economic Geology*. Society of Economic Geologists, Inc., Chelsea, MI.
- Olson, G.J. 1991. Rate of pyrite bioleaching by *Thiobacillus ferrooxidans*: Results of an interlaboratory comparison. *Applied and Environmental Microbiology*, Mar. 1991. p. 642-644.

- Plumlee, G.S. 1999. The environmental geology of mineral deposits. p. 71-116. *In* The Environmental Geochemistry of Mineral Deposits. Part A: Processes, Techniques, and Health Issues, vol. 6A, chapter 3. Reviews in Economic Geology. Society of Economic Geologists, Inc., Chelsea, MI.
- Pugh, C.E., Hossner, L.R., Dixon, J.B. 1984. Oxidation rate of iron sulfides as affected by surface area, morphology, oxygen concentration, and autotrophic bacteria. *Soil Science*, v. 137, no. 5. p. 309-314. <http://dx.doi.org/10.1097/00010694-198405000-00003>.
- Rauch, H.W., White W.B. 1977. Dissolution kinetics of carbonate rocks: 1. Effects of lithology on dissolution rate. *Water Resources Research*, v. 13, no. 2. p. 381-394. <http://dx.doi.org/10.1029/WR013i002p00381>.
- Singer, P.C., Stumm, W. 1970. Acid mine drainage: The rate determining step. *Science*, v. 167. p. 1121-1123. <http://dx.doi.org/10.1126/science.167.3921.11213>.
- Smith, K.S. 1999. Metal sorption on mineral surfaces: An overview with examples relating to mineral deposits. p. 161-182. *In* The Environmental Geochemistry of Mineral Deposits. Part B: Case Studies and Research Topics. Vol. 6B, Chapter 7. Filipek, L., Plumlee, G. (Volume Eds). Reviews in Economic Geology. Society of Economic Geologists, Inc., Chelsea, MI.
- Smith, K.S, Huyck, H.L.O. 1999. An overview of the abundance, relative mobility, bioavailability, and human toxicity of metals. p. 29-70. *In* The Environmental Geochemistry of Mineral Deposits. Part A: Vol. 6A, Chapter 2. Plumlee, G., Logsdon, M. (Volume eds.). Reviews in Economic Geology. Society of Economic Geologists, Inc., Chelsea, MI.
- Streckeisen, A. 1976. Classification of the common igneous rocks by means of their chemical composition: a provisional attempt. *Neues Jahrbuch für Mineralogie, Monatshefte*, H. 1. p. 1-15.
- Streckeisen, A. 1978. IUGS Subcommittee on the systematics of igneous rocks. Classification and nomenclature of volcanic rocks, lamprophyres, carbonatites and melilitite rocks. Recommendations and suggestions. *Neues Jahrbuch für Mineralogie, Abhandlungen*, v. 141. p. 1-14.
- Stumm, W., Morgan, J.J. 1981. Aquatic chemistry - an introduction emphasizing chemical equilibria in natural waters. John Wiley and Sons, Inc. New York. 470 p.
- White, A., Bullen, T., Vivit, D., Schulz, M., Clow, D. 1999. The role of disseminated calcite in the chemical weathering granitoid rocks. *Geochim. Cosmochim. Acta*, v. 63. p. 1939-1953. [http://dx.doi.org/10.1016/S0016-7037\(99\)00082-4](http://dx.doi.org/10.1016/S0016-7037(99)00082-4).
- White, A.F., Schulz, M.S., Lowenstern, J.B., Vivit, D.V, and Bullen T.D. 2005. The ubiquitous nature of accessory calcite in granitoid rocks: Implications for weathering, solute evolution, and petrogenesis. *Geochim. Cosmochim. Acta*, v. 69. p. 1455-1471. <http://dx.doi.org/10.1016/j.gca.2004.09.0121>.
- White, W.W. III, Jeffers, T.H. 1994. Chemical predictive modeling of acid mine drainage from metallic sulfide-bearing rock. p. 608-630. *In* Environmental Geochemistry of Sulfide

Oxidation; ACS Symposium Series 550; American Chemical Society: Washington, DC, 1993.

Williamson, M.A., Rimstidt, J.D. 1994. The kinetics and electrochemical rate-determining step of aqueous pyrite oxidation. *Geochim. Cosmochim. Acta*, v. 58. p. 5443-5454.  
[http://dx.doi.org/10.1016/0016-7037\(94\)90241-0](http://dx.doi.org/10.1016/0016-7037(94)90241-0)